# ChemComm

Accepted Manuscript


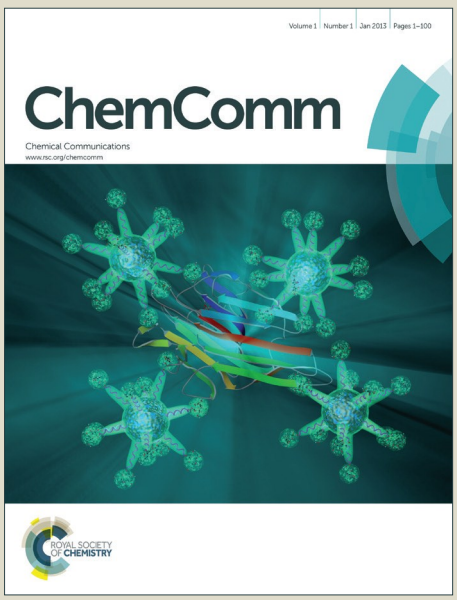





ROYAL SOCIETY OF CHEMISTRY

www.rsc.org/chemcomm

Cite this: DOI: 10.1039/c0xx00000x

www.rsc.org/xxxxxx

COMMUNICATION

# The fluorescence regulation mechanism of the paramagnetic metal in a biological HNO sensor

**Wenjing Yang,[a] Xuebo Chen,*[a] Huizhen Su,[a] Weihai Fang,[a] and Yong Zhang*[b]**

***Received (in XXX, XXX) Xth XXXXXXXXX 20XX, Accepted Xth XXXXXXXXX 20XX***

**DOI: 10.1039/b000000x**

**Paramagnetic metals are frequently used to regulate fluorescence emissions in chemical and biological probes. Accurate quantum calculations offer the first regulation theory that quenching is through the competitive nonradiative decay of the mixed fluorophore/metal $^3\pi\pi^*$/dd state isoenergetic to fluorophore-localized $^1\pi\pi^*$ state.**

Paramagnetic metal ions, such as $Cu^{2+}$, $Co^{2+}$, $Ni^{2+}$, and $Fe^{3+}$, are frequently used to quench fluorescence to facilitate *ON-OFF* signaling of interesting chemical and biological systems.[1] For instance, $[Cu^{II}(BOT1)Cl]^+$ (see Scheme 1), was recently reported as the first fluorescence probe[2] to directly detect nitroxyl (HNO), an important biological nitric oxides, in living cells. Among all the nitrogen oxides, HNO, the one-electron reduced and protonated analogue of the well-known signaling molecule nitric oxide (NO), is unique in its chemistry and biology.[3] Investigations of HNO can be traced back to early studies of fundamental physical examinations and the elucidation of interactions in atmospheric, industrial and bacterial processes in the past century.[3] The recent reports have indicated that HNO has important biological activity and pharmacological effects, such as vascular relaxation, enzyme activity regulation, neurological function regulation, enhanced cell oxidative stress, blood-brain barrier disruption, and neutrophil infiltration during renal ischemia/reperfusion.[4] Although the original study of HNO first emerged in more than 100 years ago, the understanding of the chemistry and biochemistry of HNO and its detection *in vivo* have seriously lagged behind other redox nitrogen oxide congeners.[3] To date, most HNO detection methods are indirect or inconvenient for *in vivo* uses.[5]

As an illustrative example of the direct HNO sensor, the metal's regulatory role is to quench the fluorescence of BOT1 upon $Cu^{II}$ binding, and to regenerate fluorescence by reaction with the targeting molecule, HNO, leading to metal center reduction to diamagnetic $Cu^{I}$.[2] The basic idea of using $Cu^{II}$ complex as the HNO receptor site and such redox reaction to couple with a fluorescence signaling site has been recently used to develop a few other metal-based HNO fluorescence probes.[6] Although the quenching mechanisms of paramagnetic metals are usually hypothesized to result from photoinduced electron transfer (PET) from singlet fluorophore excited state to paramagnetic metal centers,[2,6a,7] a rigorous examination of this hypothesis and related fluorescence mechanistic details has not been reported. In addition, although derivatives of the central signaling unit, 4,4-difluoro-4-bora-3a,4a-diaza-s-indacene (BODIPY), are widely used in chemical and biological studies,[8] with relatively sharp fluorescence peaks, high quantum yields, and optical properties suited for cellular imaging,[2,6a,8] their fluorescence mechanisms are yet to be reported, despite early calculations of orbital energies.[9] Here, we employed a multi-configurational quantum chemical study [see Electronic Supplementary Information (ESI) for computational details] that has been verified to be superior in investigations of excited states of various systems containing transition metals[7] to investigate $[Cu^{II}(BOT1)Cl]^+$ and related systems as the first example to elucidate a fluorescence regulation theory for paramagnetic metal systems and the associated mechanism-based design principle, based on excellent predictions of experimental absorption and fluorescence properties.

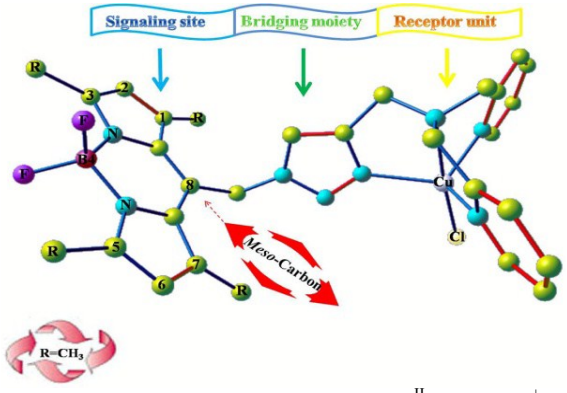


**Scheme 1**. Chemical structure of $[Cu^{II}(BOT1)Cl]^+$ with numbering and labelling schemes. Hydrogen atoms are omitted for clarity.

The central signalling unit of BOT1, 1,3,5,7,8-pentamethyl substituted BODIPY (**1**), was first studied. As shown in Fig.1, the ground state to excited state $S_0 \rightarrow S_{CT}(^1\pi\pi^*)$ transition is the lowest excitation with the largest oscillator strength ($f$=0.81). The calculated vertical excitation energy ($E_\lambda$), 2.49 eV (498 nm) is in excellent accord with the experimental maximum absorption wavelength, $\lambda_{max,abs}$ (493 nm).[8,10] The adiabatic excitation energy ($E_{0\text{-}0}$) was also shown in Table 1. A large photo-initiated charge translocation (PCT) with 0.481 *e* was found from the dimethylpyrro ring to the rest moiety (see Fig. 1 and ESI), leading to geometric inequality of this symmetrically substituted system.

As shown in Fig. 1, following the initial excitation, **1** rapidly decays to its minimum, $S_{CT}(^1\pi\pi^*)$-min, 0.41 eV below the Frank-Condon (FC) point through a flat relaxation path. A large oscillator strength ($f_{em}$=0.85) was found for the fluorescence emission, in excellent accord with the high experimental quantum yield ($\Phi$=0.99).[8,10]

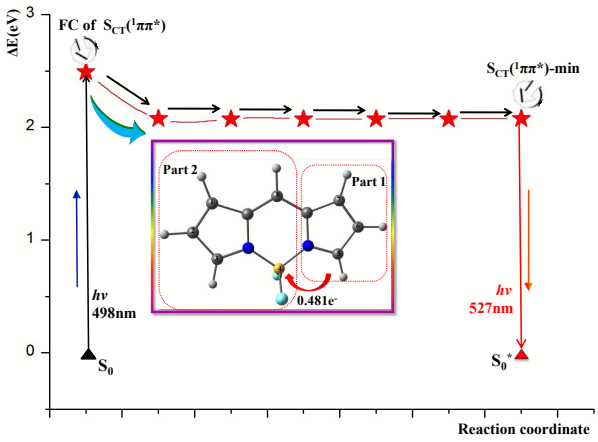


**Fig. 1** Radiative relaxation pathway for 1 with $S_{CT}(^1\pi\pi^*)$ state energies (red star points) along the relaxation pathway.

The calculated fluorescence emission wavelength ($\lambda_{FE}$), 527 nm, is also close to experiment (519 nm).[8,10] This excellent fluorescence emission provides a strong theoretical basis of the experimental application of **1** as a useful signaling unit in $[Cu^{II}(BOT1)Cl]^+$. When **1** is incorporated in BOT1, the calculated absorption peak of 523 nm is in good agreement with the experimental value of 518 nm.[2] The computed emission energy (corresponding to 565 nm) is only red shifted by 0.16 eV compared with experiment (526 nm).[2] Interestingly, these data are similar to those for **1**, suggesting a minor effect of bridge and receptor units on absorption and emission wavelengths. However, they induce a significant decrease of PCT from 0.481 *e* in **1** to 0.210 *e* in BOT1, in correlation with a large Φ decrease from 0.99 to 0.12.[2,8,9b,10] This may be a result of the electron-donating triazole group to reduce the electron-accepting capability of part 2 in the fluorescence process. These results provide the first details of the fluorescence state of the signaling site and the importance of PCT.

**Table 1**. Selected computational data for diamagnetic systems.

| System | *f* | $E_\perp$(eV) | $E_{0\text{-}0}$ | $\lambda_{FE}$(nm) |
|---|---|---|---|---|
| **1** | 0.81 | 2.49 | 2.08 | 527 |
| **BOT1** | 1.03 | 2.37 | 2.16 | 565 |
| **$[Cu^I(BOT1)]Cl$** | 0.95 | 2.42 | 2.02 | 565 |

To help understand the experimental fluorescence quenching effect of $Cu^{II}$ binding to BOT1,[2] we first briefly examined a number of excitation mechanisms of $[Cu^{II}(BOT1)Cl]^+$ shown in Table 2 with details in ESI. The lowest ground state to excited state excitation, $^2D_0\rightarrow{}^2D_1$(dd), is localized in the metal center, involving an electron transition from $d_{x^2-y^2}$ to $d_{Z^2}$, which confirms the conventional knowledge that d-d transition is a low energy excitation.[7a,11] In contrast, the second and third transitions are localized in the BODIPY part, with π→π* triplet $^2D_0\rightarrow{}^2D_2(^3\pi\pi^*)$ and singlet $^2D_0\rightarrow{}^2D_3(^1\pi\pi^*)$ excitations, respectively. The singlet transition is predicted to be the strongest absorption due to the largest calculated oscillator strength (Table 2). The computed absorption peak (544 nm) is close to experiment (518 nm).[2] The similarity of calculated $E_\perp$ and *f* data to those of BOT1 suggests that $^2D_3(^1\pi\pi^*)$ is responsible for the initial excitation and a reddish emission from the BODIPY unit might occur afterwards.

However, there is a nearly isoenergetic FC excitation (2.32 vs. 2.28eV), $^2D_0\rightarrow{}^2D_{3'}(^3\pi\pi^*/dd)$, where two unpaired electrons occupy the BODIPY π/π* orbitals identical to that in $^2D_2(^3\pi\pi^*)$, and the third unpaired electron populates in the same metal d excited state as in $^2D_1$(dd). This mixed excitation nature is further confirmed by $E_\perp$'s for these three FC transitions, since $E_\perp$ of $^2D_0\rightarrow{}^2D_{3'}(^3\pi\pi^*/dd)$ equals to the sum of $E_\perp$'s for $^2D_0\rightarrow{}^2D_2(^3\pi\pi^*)$ and $^2D_0\rightarrow{}^2D_1$(dd), see Table 2. In addition, this mixed excitation character is evident in the minimum structure of $^2D_{3'}(^3\pi\pi^*/dd)$ where bond parameters of BODIPY moiety resemble those of $^2D_2(^3\pi\pi^*)$ state minimum, and the elongated Cu-N/Cu-Cl bonds along $d_{Z^2}$ orbital direction bear similarity with the character of structural changes of d-d transition (see ESI).

**Table 2.** Selected computational data for $[Cu^{II}(BOT1)Cl]^+$.

| Transitions | Vertical | | Adiabatic | Singly occupied orbitals |
|---|---|---|---|---|
| | *f* | $E_\perp$ | $E_{0\text{-}0}$ | |
| $^2D_0$ | | 0 | | $d_{Z^2}$ |
| $^2D_0\rightarrow{}^2D_1$(dd) | $<10^{-5}$ | 0.76 | 0.65 | $d_{x^2-y^2}$ |
| $^2D_0\rightarrow{}^2D_2(^3\pi\pi^*)$ | $<10^{-8}$ | 1.56 | 1.16 | π $d_{Z^2}$ π* |
| $^2D_0\rightarrow{}^2D_3(^1\pi\pi^*)$ | 1.20 | 2.28 | 2.02 | π $d_{Z^2}$ π* |
| $^2D_0\rightarrow{}^2D_{3'}(^3\pi\pi^*/dd)$ | $<10^{-8}$ | 2.32 | 1.98 | π $d_{x^2-y^2}$ π* |
| $^2D_0\rightarrow{}^2D_{LMCT}(\pi d)$ | $<10^{-5}$ | -- | 1.51 | π |

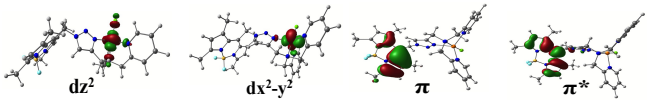


This mixture pattern was also found in another $Cu^{II}$-based sensor,[7a] suggesting that it may be general for fluorescence unit-$Cu^{II}$ complexes. An important consequence is to provide a bypass channel to quench fluorescence emission (*vide infra*). In addition, a π→d transition, $^2D_0\rightarrow{}^2D_{LMCT}(\pi d)$, between the BODIPY moiety and the $Cu^{2+}$ center was found to be ~0.8 eV lower than the above isoenergetic transitions. This makes the electron communication between metal and fluorescence unit energetically favorable to regulate the nonradiative relaxation (*vide infra*). It also supports the significance of PET from the fluorescence site to the metal center repeatedly implied/speculated in experimental studies,[1,12] which, however, was found here to be only part of the full mechanism.

The key decay processes from the joint FC region of isoenergetic $^2D_{3'}(^3\pi\pi^*/dd)$ and $^2D_3(^1\pi\pi^*)$ are shown in Fig. 2 with more details in ESI. Although the fluorescent $^2D_3(^1\pi\pi^*)$ state is most possibly to be initially populated due to its largest oscillator strength (Table 2), luminous relaxation is slow with a ns timescale (0.15 ns),[2] which cannot compete with the ultrafast nonradiative decay of the isoenergetic $^2D_{3'}(^3\pi\pi^*/dd)$ state (*vide infra*). Therefore, the $^2D_{3'}(^3\pi\pi^*/dd)$ state governs the dominant decay channel through direct initial population to this state or an effective internal conversion of $^2D_3(^1\pi\pi^*)\rightarrow{}^2D_{3'}(^3\pi\pi^*/dd)$ in the isoenergetic FC region. This explains the considerably low experimental Φ (0.01).[2]

As shown in Fig. 2 and ESI, the initial decay of $^2D_{3'}(^3\pi\pi^*/dd)$ is associated with structural changes in both BODIPY and $Cu^{II}$ center, resembling those for $^2D_{3'}(^3\pi\pi^*/dd)$-min with the characteristics of mixed $^3\pi\pi^*/dd$ excitation. It then rapidly decays to the conical intersection, **CI**($^2D_{3'}/^2D_2$), between $^2D_{3'}(^3\pi\pi^*/dd)$ and $^2D_2(^3\pi\pi^*)$ with a 0.17 eV energy decrease. The energy gap between two excited states at CI($^2D_{3'}/^2D_2$) is calculated to be only 0.082 eV. Such strong non-adiabatic coupling allows a fast interconversion to occur effectively from $^2D_{3'}(^3\pi\pi^*/dd)$ to

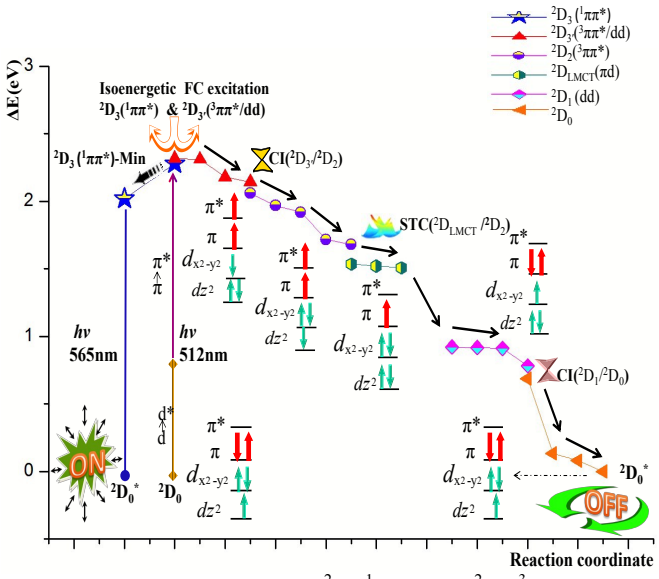


**Fig. 2** Decay pathways from $^2D_3(^1\pi\pi^*)$ vs. $^2D_3(^3\pi\pi^*/dd)$ of $[Cu^{II}(BOT1)Cl]^+$.

$^2D_2(^3\pi\pi^*)$ state. Meanwhile, axial Cu-Cl and Cu-N bonds are elongated to be 2.363 and 2.253 Å in **CI**($^2D_3/^2D_2$) compared with those (2.324/2.199 Å) in the $^2D_0$ ground state, but are shorter than those in the $^2D_3(^3\pi\pi^*/dd)$-min excited state (see ESI), suggesting that **CI**($^2D_3/^2D_2$) is an intermediate to approach ground state structure for the moiety of $Cu^{II}$ center. It also functions as an effective nonadiabatic relay to repopulate the unpaired electron of $Cu^{II}$ from $d_{x^2-y^2}$ to $d_{Z^2}$ to help recover its ground state electronic structure, allowing an ultrafast decay to $^2D_2(^3\pi\pi^*)$ state, in which the excited state pattern now becomes centered on BODIPY only. The evolution of $^2D_2(^3\pi\pi^*)$ along a slightly downhill energy path then reaches the singlet triplet crossing between $^2D_2(^3\pi\pi^*)$ and $^2D_{LMCT}(\pi d)$, referred as STC($^2D_{LMCT}/^2D_2$) in Fig. 2. The small energy difference (0.144 eV) and strong spin-orbit coupling at STC($^2D_{LMCT}/^2D_2$) enable the $^2D_2 \rightarrow {}^2D_{LMCT}$ transition with high efficiency in the subpicosecond timescale,[13] facilitated by the electron transfer from the high energy BODIPY π* orbital to the low energy $Cu^{II}$ $d_{Z^2}$ orbital. This type of π → d electron communication induces the weakened axial Cu-Cl and Cu-N bonds (~2.50 Å) around the $Cu^{2+}$ center, besides the retention of the excited BODIPY triplet state structural character (see ESI). Consistently, dipole moment increases significantly to ca. 30 Debye in STC($^2D_{LMCT}/^2D_2$) from ca. 15 Debye in $^2D_2(^3\pi\pi^*)$. This triggers the electron repopulation to recover the BODIPY ground state structure by a reverse electron transfer from $d_{x^2-y^2}$ to the π orbital leading to the double occupancy of the BODIPY π orbital, which is much more stable than $^2D_{LMCT}(\pi d)$. This generates the $^2D_1(dd)$ state, e.g. the axial Cu-Cl and Cu-N bonds are further shortened to 2.320 and 2.298Å from ~2.50 Å in $^2D_{LMCT}(\pi d)$-min. **CI**[$^2D_1(dd)/^2D_0$] was found to seam the surface between $^2D_1(dd)$ and the ground state. It is 0.73 eV lower than $^2D_{LMCT}(\pi d)$-min, acting as an effective relay by switching the unpaired electron from $d_{x^2-y^2}$ to $d_{Z^2}$. The closeness of the energy levels (0.095 eV) ensures **CI**[$^2D_1(dd)/^2D_0$] to function as an effective non-adiabatic funnel by the enhanced non-adiabatic coupling between dd and ground states. With the electron repopulation, the ground state recovery is achieved by the changes of axial Cu-Cl and Cu-N bonds in a similar downhill pathway to its hot ground state ($^2D_0$*) with high efficiency. In this way, this non-radiative decay competitively shuts off the fluorescence emission channel.

These results for the first time show that quenching is primarily based on the efficient conversion from the fluorescent $^2D_3(^1\pi\pi^*)$ state to the mixed state of $^2D_3(^3\pi\pi^*/dd)$ due to close energy proximity and the subsequent ultrafast downhill decay of this mixed state, not the widely reported experimental hypothesis[4] of only electron transfer from fluorophore singlet excited state to $Cu^{II}$. In fact, as shown in Fig. 2, both the forward and backward electron transfers from fluorophore to metal are important for the non-radiative decay, along with other localized changes. The close energy proximity of the fluorescent state and non-fluorescent state was also found to be an important feature of quenching effect in non-metal systems, e.g. fluorescent $^1\pi\pi^*$ state vs. non-fluorescent $^1n\pi^*$ state.[7a] This suggests that close energy proximity facilitates the conversion from the fluorescent state to the non-fluorescent state via energy resonance. Our results thus offer the first mechanism-based design principle for such systems: the metal d-d transition energy shall be close to the singlet-triplet splitting of the fluorophore to result in almost isoenergetic $^1\pi\pi^*$ state and the mixed $^3\pi\pi^*$/dd state.

Experimental results show that upon the introduction of HNO to the solution of $[Cu^{II}(BOT1)Cl]^+$, the copper center is reduced to Cu(I) with the concomitant release of NO.[2] Since the HNO/NO conversion mechanism via the reduction of $[Cu^{II}(BOT1)Cl]^+$ has been investigated in our previous work,[14] herein we focus to understand how the reduced metal complex restores the fluorescence of the BODIPY unit that is quenched in the oxidized Cu(II) system. In $[Cu^{I}(BOT1)]Cl$, the $Cu^+$ atom with a completely filled $d^{10}$ electronic configuration is penta-coordinated by four nitrogen atoms from the triazole bridge and tripodal dipicolylamine, and $Cl^-$, see ESI. There are four weak Cu-N bonds with bond lengths of 2.22–2.48Å in the ground state of the $[Cu^{I}(BOT1)]Cl$ complex. Upon photo-excitation of $S_0 \rightarrow S_{CT}(^1\pi\pi^*)$, these Cu-centered bond lengths remain almost unchanged, while significant structural changes mainly take place in the BODIPY moiety. This suggests that the perturbation to the excited state properties of BOT1 from $Cu^+$ ($d^{10}$) binding is negligible. Indeed, as shown in Table 1, the fluorescence emission wavelength is predicted to be the same as in BOT1. As a result, the reddish fluorescence emission is re-generated from the BODIPY moiety when $[Cu^{II}(BOT1)Cl]^+ \rightarrow [Cu^{I}(BOT1)]Cl$ conversion occurs in the presence of HNO, which is in excellent agreement with experiment.[2]

The solvent effect has also been examined to inspect how solvent polarity or microenvironment influences the radiative/non-radiative mechanism (see ESI). It was found that these factors may slightly alter the energy level but unlikely modifies the basic mechanism of the competitive non-radiative relaxation through energy resonance, although solvent polarity may accelerate the PET from the fluorescence site to the metal center, a part of the full mechanism described in this work.

In summary, the most important discovery from this work is the fluorescence regulation theory for paramagnetic metal systems due to the competitive nonradiative decay of the mixed fluorophore/metal $^3\pi\pi^*$/dd state isoenergetic to fluorophore-localized $^1\pi\pi^*$ state, which will help understand other similar sensors and facilitate mechanism-based design for chemical and biological applications.

This work was supported by NSFC21373029 to X.B.C., Major State Basic Research Development Programs 2011CB808503 to W.H.F., and an NIH grant GM085774 to YZ.

## Notes and references

[a]*Key Laboratory of Theoretical and Computational Photochemistry of Ministry of Education, Department of Chemistry, Beijing Normal University, Xin-wai-da-jie No. 19, Beijing, 100875, People's Republic of China, Email: xuebochen@bnu.edu.cn*

[b]*Department of Chemistry, Chemical Biology, and Biomedical Engineering, Stevens Institute of Technology, Castle Point on Hudson, Hoboken, New Jersey 07030, Unites States. Email: yong.zhang@stevens.edu*

†Electronic Supplementary Information (ESI) available: Computational details, Figures, Tables and Cartesian Coordinates. See DOI:10.1039/b000000x/


1. (a) H. S. Jung, P. S. Kwon, J. W. Lee, J. I. Kim, C. S. Hong, J. W. Kim, S. Yan, J. Y. Lee, J. H. Lee, T. Joo and J. S. Kim, *J. Am. Chem. Soc*., 2009, **131**, 2008–2012; (b) S. Pal, N. Chatterjee and P. K. Bharadwaj, *RSC Adv*., 2014, **4**, 26585–26620; (c) A. W. Varnes, R. B. Dodson and E. L. Wehry, *J. Am. Chem. Soc*., 1972, **94**, 946-950.
2. J. Rosenthal and S. J. Lippard, *J. Am. Chem. Soc*., 2010, **132**, 5536-5537.
3. (a) L. J. Ignarro, et al. Nitric oxide: biology and pathobiology, 2nd edition, ed. L. J. Ignarro, (Academic, San Diego), 2010; (b) J. M. Fukuto, C. H. Switzer, K. M. Miranda and D. A. Wink, *Annu. Rev. Pharmacol. Toxicol*., 2005, **45**, 335–355; (c) K. M. Miranda, *Coord. Chem. Rev*., 2005, **249**, 433−455; (d) Y. Gao, A. Toubaei, X. Q. Kong and G. Wu, *Angew. Chem. Int. Ed*., 2014, **53**, 11547 – 11551; (e) A. L. Speelman and N. Lehnert, *Angew. Chem. Int. Ed*., 2013, **52**, 12283 –12287.
4. (a) N. Paolocci, W. F. Saavedra, K. M. Miranda, C. Martignani, T. Isoda, J. M. Hare, M. G. Espey, J. M. Fukuto, M. Feelisch, D. A. Wink and D. A. Kass, *Proc. Natl. Acad. Sci. U.S.A*., 2001, **98**, 10463−10468; (b) N. Paolocci, T. Katori, H. C. St. Champion, M. E. John, K. M. Miranda, J. M. Fukuto, D. A. Wink and D. A. Kass, *Proc. Natl. Acad. Sci. U.S.A*., 2003, **100**, 5537−5542; (c) M. Feelisch, *Proc. Natl. Acad. Sci. U.S.A*., 2003, **100**, 4978−4980. (d) R. Smulik, D. Dębski, J. Zielonka, B. Michałowski, J. Adamus, A. Marcinek, B. Kalyanaraman and A. Sikora, *The Journal of Biological Chemistry.,* 2014, **289**, 35570-35581. (e) J. F. DuMond and S. B. King, *Antioxidants & Redox Signaling*., 2011, **14**, 1637-1648.
5. (a) N. I. Butkovskaya, A. A. Muravyov and D. W. Setser, *Chem. Phys. Lett*., 1997, **266**, 223−226. (b) M. R. Cline, C. Tu, D. N. Silverman and J. P. Toscano, *Free Radical., Biol. Med.* 2011, **50**, 1274−1279. (c) G. J. Mao, X. B. Zhang, X. L. Shi, H. W. Liu, Y. X. Wu, L. Y. Zhou, W. H. Tan and R. Q. Yu, *Chem. Commun*., 2014, **50**, 5790-5792. (d) X. T. Jing, F. B. Yu and L. X. Chen, *Chem. Commun*., 2014, **50**, 14253-14256.(e) J. A. Reisz, C. N. Zink and S. B. King, *J. Am. Chem. Soc.,* 2011, **133**, 11675−11685. (f) M. R. Cline and J. P. Toscano, *J. Phys. Org. Chem*., 2011, **24**, 993−998.
6. (a) A. T. Wrobel, T. C. Johnstone, A. Deliz Liang, S. J. Lippard and P. Rivera-Fuentes, *J. Am. Chem. Soc*., 2014, **136**, 4697−4705; (b) U. P. Apfel, D. Buccella, J. J. Wilson and S. J. Lippard, *Inorg. Chem*., 2013, **52**, 3285−3294; (c) Y. Zhou, K. Liu, J. Y. Li, Y. Fang, T. C. Zhao and C. Yao, *Org. Lett*., 2011, **13**, 1290–1293; (d) Z. P. Liu, W. J. He and Z. J. Guo, *Chem. Soc. Rev*., 2013, **42**, 1568-1600.
7. (a)H. Z. Su, X. B. Chen and W. H. Fang, *Anal. Chem*., 2014, **86**, 891−899; (b) J. Han, X. B. Chen, L. Shen, Y. Chen, W. H. Fang and H. B. Wang, *Chem. Eur. J*., 2011, **17**, 13971-13977; (c) J. Han, L. Shen, X. B. Chen and W. H. Fang, *J. Mater. Chem. C*., 2013, **1**, 4227-4235.
8. A. Loudet and K. Burgess, *Chem. Rev*., 2007, **107**, 4891–4932.
9. (a) Y. Gabe, Y. Urano, K. Kikuchi, H. Kojima and T. Nagano, *J. Am. Chem. Soc*., 2004, **126**, 3357-3367; (b) H. Lu, J. Mack, Y. Yang and Z. Shen, *Chem. Soc. Rev*., 2014, **43**, 4778-4823.
10. G. Sathyamoorthi, J. H. Boyer, T. H. Allik and S. Chandra, *Heteroat. Chem*., 1994, **5**, 403-407.
11. (a) M. Q. Zhao, L. Sun and R. M. Crooks, *J. Am. Chem. Soc*., 1998, **120**, 4877−4878; (b) B. C. Larson, W. Ku, J. Z. Tischler, C. C. Lee, O. D. Restrepo, A. G. Eguiluz, P. Zschack and K. D. Finkelstein, *Phys. Rev. Lett*., 2007, **99**, 026401-026404; (c) A. R. Amundsen, J. Whelan and B. Bosnich, *J. Am. Chem. Soc*., 1977, **99**, 6730−6739.
12. (a) L. Y. Niu, Y. S. Guan, Y. Z. Chen, L. Z. Wu, C. H. Tung and Q. Z. Yang, *J. Am. Chem. Soc*., 2012, **134**, 18928−18931; (b) X. J. Wu, H. D. Li, Y. H. Kan and B. Z. Yin, *Dalton Trans*., 2013, **42**, 16302-16310; (c) L. Y. Niu, Y. S. Guan, Y. Z. Chen, L. Z. Wu, C. H. Tung and Q. Z. Yang, *Chem. Commun*., 2013, **49**, 1294-1296.
13. (a) V. F. Plyusnin, I. P. Pozdnyakov, V. P. Grivin, A. I. Solovyev, H. Lemmetyinen, N. V. Tkachenko and S. V. Larionov, *Dalton Trans*., 2014, **43**, 17766–17774; (b) M. D. Allendorf, C. A. Bauer, R. K. Bhakta and R. J. T. Houk, *Chem. Soc. Rev*., 2009, **38**, 1330–1352.
14. M. A. Michael, G. Pizzella, L. Yang, Y. Shi, T. Evangelou, D. T. Burke and Y. Zhang, *J. Phys. Chem. Lett*., 2014, **5**, 1022−1026.


## Graphic Abstract

A theoretical model was developed to reveal the origin of paramagnetic metal induced fluorescence quenching.